



# Controlling a crystalline seed layer for microcrystalline silicon oxide window layer in rear emitter silicon heterojunction cells

Duy Phong Pham<sup>a</sup>, Sangho Kim<sup>b</sup>, Sunhwa Lee<sup>a</sup>, Anh Huy Tuan Le<sup>c,d</sup>, Eun-Chel Cho<sup>a</sup>, Jinjoo Park<sup>e,\*</sup>, Junsin Yi<sup>a,\*</sup>

<sup>a</sup> College of Information and Communication Engineering, Sungkyunkwan University, 2066 Seobu-ro, Suwon-si, Gyeonggi-do 16419, Republic of Korea

<sup>b</sup> Department of Energy Science, Sungkyunkwan University, 2066 Seobu-ro, Suwon-si, Gyeonggi-do 16419, Republic of Korea

<sup>c</sup> Division of Computational Physics, Institute for Computational Science, Ton Duc Thang University, Ho Chi Minh City, Viet Nam

<sup>d</sup> Faculty of Electrical and Electronics Engineering, Ton Duc Thang University, Ho Chi Minh City, Viet Nam

<sup>e</sup> Major of Energy and Applied Chemistry, Division of Energy & Optical Technology Convergence, Cheongju University, Republic of Korea

## ARTICLE INFO

### Keywords:

Seed crystals  
Chemical vapor deposition processes  
Semiconducting silicon compounds  
Silicon heterojunction solar cells

## ABSTRACT

Remarkable progress has been made in the improvement of rear-emitter silicon heterojunction (RE-SHJ) solar cells with the use of very thin n-type front contact layers. However, further reducing the thickness of the front window layers while maintaining high conductivity for mitigating the parasitic absorption and carrier collection loss has proven challenging. In this study, we implement controlling a seed layer for achieving ultra-thin, high crystalline and conductivity of n-type hydrogenated microcrystalline silicon oxide (n- $\mu\text{c-SiO}_x\text{:H}$ ) front window layer in RE-SHJ solar cells. By using a seed layer, the crystallinity confirmed by Raman and TEM measurements, and the conductivity of the n- $\mu\text{c-SiO}_x\text{:H}$  front layers are significantly enhanced compared with that without using the seed layer. This leads to a remarkable increase in the open-circuit voltage ( $V_{oc}$ ) by 6 mV and fill factor ( $FF$ ) by 4.11% while maintaining a high short-circuit current density ( $J_{sc}$ ) in range of 38 mA/cm<sup>2</sup>. A high cell performance of 21.1% is obtained with the use of an optimised seed layer.

## 1. Introduction

Silicon heterojunction (SHJ) solar cells have received a lot of attention owing to their advantages such as high efficiencies with the use of a simple and cost-effective production process [1,2]. The excellent surface passivation of SHJs is one of the important advancements made, which can lead to very high open-circuit voltages ( $V_{oc}$ ) and a significantly simple fabrication process without requiring any additionally complex patterning steps [3]. For competitive cost-effective photovoltaic applications, persistent efforts have mainly focused on further improving cell performance [4,5]. The main performance limitation of SHJ cell type compared with their counterpart solar cells such as the interdigitated back contact (IBC) or passivated emitter rear contact (PERC) cells has been attributed to the parasitic absorption of the front layers that are stacked together, such as passivation, doping front contact, and transparent conductive oxide (TCO) layers [6,7]. Consequently, efforts have been made to optimize the front-layer stack, mainly focusing on sufficient doping and achieving thinner layers [6,8].

Traditionally, p-type emitter layers have been used at the front side to efficiently collect minority charge carriers owing to the shortest

carrier diffusion paths [3]. However, because of the inherent poor conductivity compared with its n-type counterpart, a higher doping and/or a thicker p-type layer may be required to maintain an internal electrical field for sufficient hole-collection [6,9]. A thicker and/or a higher doped p-type layer can result in both more significant parasitic absorption and junction recombination which can lead to impair  $V_{oc}$ , short-circuit current density ( $J_{sc}$ ) and fill factor ( $FF$ ). Moreover, a Schottky barrier can be formed between the window layer (p-type) and n-type front TCOs in case of insufficient doping and/or thinner p-layers [10,11]. To overcome these limitations, RE-SHJ cells that use the p-type emitter at the rear side of the cell are proposed as a potential configuration [12–14]. The long minority carrier lifetime (several milliseconds) in the current high-quality n-type silicon wafers offers promising potential for the utility of p-type emitters at the back side without significant collection losses. In addition, the use of the RE-SHJ structure leads to fewer restrictions in choosing TCO materials and particularly enhances more transparent front stacks because an n-type front contact layer can be made thinner than its p-type counterpart without significant conductivity losses [15,16].

Phosphorous doped hydrogenated microcrystalline silicon-oxide (n-

\* Corresponding authors.

E-mail addresses: [pdphong@skku.edu](mailto:pdphong@skku.edu) (D.P. Pham), [lehuytuananh@tdtu.edu.vn](mailto:lehuytuananh@tdtu.edu.vn) (A.H.T. Le), [jwjh3516@cju.ac.kr](mailto:jwjh3516@cju.ac.kr) (J. Park), [junsin@skku.edu](mailto:junsin@skku.edu) (J. Yi).

<https://doi.org/10.1016/j.infrared.2019.103037>

Received 5 July 2019; Received in revised form 9 September 2019; Accepted 9 September 2019

Available online 10 September 2019

1350-4495/© 2019 Elsevier B.V. All rights reserved.

$\mu\text{-SiO}_x\text{:H}$ ) material has been suggested as a promising front window layer for RE-SHJ cells [17,18]. It is known as a two-phase material including a columnar nanocrystalline silicon phase embedded in a matrix of amorphous silicon oxide (a-SiO<sub>x</sub>:H) phase. In such a material, the crystalline phase can provide highly vertical conductivity while the a-SiO<sub>x</sub>:H phase can enhance transparency [19,20]. Using n- $\mu\text{-SiO}_x\text{:H}$  front window layer in RE-SHJ solar cells, an impressively higher efficiency compared with an n-type hydrogenated microcrystalline silicon (n- $\mu\text{-Si:H}$ ) and amorphous silicon (n-a-Si:H) is reported [17,18]. The challenge in using n- $\mu\text{-SiO}_x\text{:H}$  at the front side in RE-SHJ structure is the deposition of a thin and high-crystalline n-type layer, i.e. high conductivity, on top of the very thin amorphous passivation (a-Si:H) membrane, without harming the under a-Si:H layer and/or passivation quality [16]. A potential solution is to boost fast the initial nucleation formation during the crystal-growth period of n- $\mu\text{-SiO}_x\text{:H}$  layer [16].

In this work, therefore, we report crystalline-seed layer (CSL) optimisation for the ultra-thin front contact n- $\mu\text{-SiO}_x\text{:H}$  layer. The CSL is prepared between the a-Si:H passivation and n- $\mu\text{-SiO}_x\text{:H}$  layers in high hydrogen content dilution without CO<sub>2</sub> content dilution to faster nucleation. Plasma source power density of the seed layer is varied in a large range of 42–214 mW/cm<sup>2</sup> to determine the optimized point. The characteristics of RE-SHJ solar cells implemented under various seed layers are discussed.

## 2. Experiment

The RE-SHJ cells were carried out on n-type pyramid-textured Czochralski wafers (with thickness of 140  $\mu\text{m}$ , size of 4 cm  $\times$  4 cm and 4.3  $\Omega\text{-cm}$  of resistivity) using a cluster multi-chamber plasma-enhanced chemical vapor deposition (PECVD) system (SNTTEK). Beforehand, the wafers were chemically textured at both surfaces in a dilute alkaline solution to obtain random pyramid-shapes with average heights of around 10  $\mu\text{m}$ . Prior the PECVD depositions, the wafers were cleaned using a standard RCA procedure and then dipped in hydrofluoric acid (1%) to remove the chemical silicon-oxide film. The PECVD deposition began with a 5 nm thick a-Si:H passivation layer on both sides of the wafer surface. A 3 nm thick CSL and a 10 nm thick n- $\mu\text{-SiO}_x\text{:H}$  layer were then deposited in the front side. The deposition condition of these layers is shown in Table 1. Boron doped hydrogenated amorphous silicon (p-a-Si:H) was subsequently deposited in the rear side. Indium-doped tin oxide (ITO) layers at both sides were then deposited using sputtering method. Prior to the ITO deposition, a rectangular-shaped metal mask was attached to the surface of the cell to calibrate the cell area of 10.24 cm<sup>2</sup>. Ag-grid electrodes were screen-printed on the front side and entirely covered at the back side of the cell. The cross-section of cell structures is illustrated in Fig. 1. Four cells were implemented in same deposition condition for each variation. All cells were characterized using a standard one-sun illumination (100 mW/cm<sup>2</sup>, AM 1.5G, at 25 °C).

The n- $\mu\text{-SiO}_x\text{:H}$  single-layers with and without CSLs were prepared on Eagle glass substrates and bare polished wafers. The deposition conditions of these layers are listed in Table 1. The crystalline phase of

**Table 1**  
Deposition parameters of seed and n- $\mu\text{-SiO}_x\text{:H}$  front layers.

Parameters	Seed layer	n- $\mu\text{-SiO}_x\text{:H}$ front
[H <sub>2</sub> ]/[SiH <sub>4</sub> ] flow ratio	160	125
[PH <sub>3</sub> ]/[SiH <sub>4</sub> ] flow ratio	1.0	2
[CO <sub>2</sub> ]/[SiH <sub>4</sub> ] flow ratio	0	0.5
Power density (mW/cm <sup>2</sup> )	42–214	42
Working Pressure (Torr)	1.5	1.5
Deposition temperature (°C)	110	110
Thickness (nm)	3	10

these films was detected by Raman measurement (Dongwoo Optron system) with a 514.5-nm-wavelength of Ar<sup>+</sup>-ion laser source. From Raman data, the crystalline volume fractions ( $X_c$ ) were calculated as following:  $X_c = I_{518}/(I_{518} + I_{480})$  where I symbol denotes the integrated area of a peak and the subscript numbers denote the wavenumber of peak. In addition, the transmission electron microscopy (TEM – JEM 2100F) system was used to identify the crystallinity of films on the polished wafer. Electrical property measurement such as conductivity using the programmable Keithley 617 electrometer was implemented using two evaporated Al coplanar electrodes on the film-surface. The activation energy ( $E_a$ ) was calculated based on the temperature-dependent dark-conductivity measurement following the Arrhenius relationship [21]. The film thickness measurement was conducted from fitting of the spectroscopic ellipsometry measurement using the J. A. Woollam VASE system.

## 3. Result and discussion

The CSLs were prepared by varying the plasma source power density from 42 to 214 mW/cm<sup>2</sup> as shown in Table 1. The seed- and front window-layer thicknesses were maintained at 3 and 10 nm, respectively. The seed layers were implemented in higher hydrogen dilution than the front window layers without CO<sub>2</sub> gas content to strongly enhance the crystalline growth [22]. Fig. 2 shows the structural property detected by Raman spectra of the front window n- $\mu\text{-SiO}_x\text{:H}$  single-layers. The  $X_c$  and conductivity of these films are summarized in Table 2. It is apparent that a thin n- $\mu\text{-SiO}_x\text{:H}$  layer without a CSL (sample A) has a weak crystalline phase with low  $X_c$  of 5%, characterised by a low intensity peak at 518 cm<sup>-1</sup> and a prevalent amorphous phase represented by the high broad peak centred at 480 cm<sup>-1</sup>. Raman characteristic of sample B with the onset of a CSL at 42 mW/cm<sup>2</sup> power density shows a sharp high-intensity peak at 518 cm<sup>-1</sup> with high  $X_c$  of 60% which characterizes a strong crystalline phase. However, the crystalline phase tended to gradually decrease with the power density, as shown in Raman spectra of samples C–E in Fig. 2 and the  $X_c$  values listed in Table 2. We can reasonably assume that high-crystalline-phase formation (sample B) can cause the conductivity three orders of magnitude higher than that of sample A. The conductivity tended to significantly decrease with the higher source power density of the seed layers. This evidence points to the likelihood that the crystalline quality or conductivity of the front window n- $\mu\text{-SiO}_x\text{:H}$  layer can be substantially enhanced by a CSL which was prepared at low power density. For corresponding with the conductivity (Table 2) and crystalline (Fig. 2) characteristics of the n- $\mu\text{-SiO}_x\text{:H}$  single-layers on polished surfaces of glass substrates, we chose identical flat surfaces of polished wafers to identify the crystallinity of these single-layers via TEM measurement although we used the textured surface of wafers for device fabrication. A cross-section TEM image of samples on the polished wafer are illustrated in Fig. 3. It shows clearly that columnar large crystalline grains (red lines) are detected densely at sample B and less at sample C including a few small crystalline grains. It seems to be difficult to detect the crystalline grains at sample A and D. In addition, in sample B, the crystalline grains seem to stem from nucleation which is deposited at low power density of 42 mW/cm<sup>2</sup>. The crystal grains were absent from sample A possibly due to the thin thickness of 10 nm of n- $\mu\text{-SiO}_x\text{:H}$  front layer. Generally, with a high [H<sub>2</sub>]/[SiH<sub>4</sub>] gas ratio (hydrogen dilution) maintained stably throughout n- $\mu\text{-SiO}_x$  deposition process, the microcrystalline phase will form after an initial incubation (amorphous phase) process [23]. Thus, a thin layer of 10 nm with the constant hydrogen dilution condition in sample A was possibly insufficient to overcome the incubation process. In the literature, to prompt fast nucleation process, different process parameter adjustments during deposition are proposed. For example, Yue et al. [24]

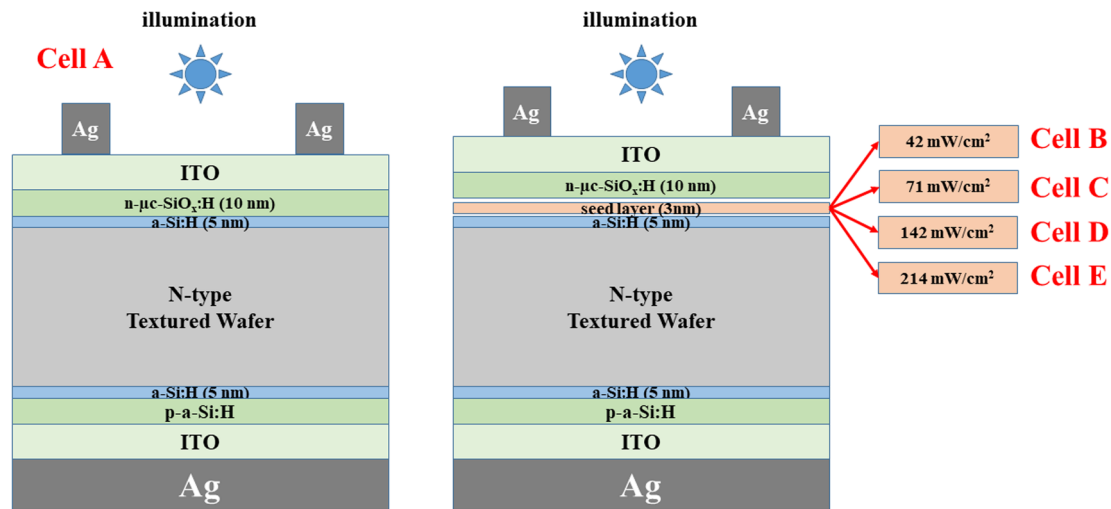


Fig. 1. The rear-emitter SHJ solar cell structure with various seed layer conditions.

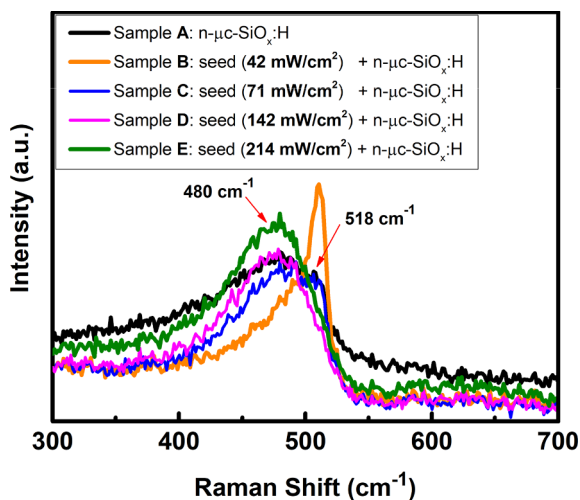


Fig. 2. Raman spectroscopies of  $n\text{-}\mu\text{c-SiO}_x\text{:H}$  front layers on various seed layer conditions.

Table 2

Conductivity, activation energy and crystalline volume factor of  $n\text{-}\mu\text{c-SiO}_x\text{:H}$  front layers on various seed layers.

Samples	Deposition power density of seed layer ( $\text{mW}/\text{cm}^2$ )	Conductivity ( $\text{S}/\text{cm}$ )	Activation energy (eV)	Crystalline volume fraction (%)
A	Without seed	$8.1 \times 10^{-5}$	0.29	5
B	42	$6.2 \times 10^{-2}$	0.08	60
C	71	$1.0 \times 10^{-3}$	0.15	10
D	142	$8.8 \times 10^{-6}$	0.31	0.3
E	214	$1.8 \times 10^{-6}$	0.34	0.1

proposed a two-step method to grow microcrystalline silicon including an ultrathin Si film first followed by hydrogen plasma treatment and deposition of  $\mu\text{c-Si:H}$  last. Chung et al. [25] suggested a HCl gas addition during initial growth stage of  $\mu\text{c-Si:H}$  film to reduce the amorphous incubation layer. Herein, as shown in Table 1, we prepared the seed layers at the  $[\text{H}_2]/[\text{SiH}_4]$  flow ratio as high as 160 with  $\text{CO}_2$  gas absence and controlled the crystallinity of these layers by varying the power

densities. As seen in Fig. 3, the nucleation process at sample B can be enhanced in low power density condition of  $42 \text{ mW}/\text{cm}^2$ ; as a result, the strongly crystalline-phase growth. However, as seen in TEM images of sample C and D, the increase in power density over  $42 \text{ mW}/\text{cm}^2$  can impair the nucleation process and as a result weak crystallinity growth of  $n\text{-}\mu\text{c-SiO}_x\text{:H}$  layer. The disrupted crystal nucleation formation when the power density is increased can be due to the bombardment of high energy ions on film surface during the growth. Kondo et al. [26] showed the significant decrease in Raman crystallinity ( $X_c$ ) with the bombarding ion energy on surface of growing film. In addition, Matsuda [27] indicated the significant decrease in crystal size and  $X_c$  when RF power density increased. Furthermore, it is important to notice that the bombarding ion energy would affect not only the nucleation of the front window layer but also the passivation quality of the a-Si:H passivation layer underneath.

To clearly illustrate this point, we deposited the seed layers without the bulk  $n\text{-}\mu\text{c-SiO}_x\text{:H}$  layer on one side of symmetrically passivated textured wafers. We used the minority-carrier lifetime measurement as initially rough parameters to estimate the passivation quality of the resulting wafer surface. Fig. 4a shows the effective minority carrier lifetime data of the initial passivated wafer (PW) without seed layer and wafers with various seeds. Fig. 4b shows the lifetime and implied  $V_{oc}$  values calculated at one-sun illumination. We found that the lifetime value as compared with that of PW enhanced significantly after seed layer deposition at  $42 \text{ mW}/\text{cm}^2$  of power density but deteriorated at higher power density up to  $214 \text{ mW}/\text{cm}^2$ . The trend of implied  $V_{oc}$  values as a function of power densities are analogous to that of lifetime values. In agreement with our previous intuitive assumption, the lifetime degradation at a power density of as high as  $214 \text{ mW}/\text{cm}^2$  could be due to the strong bombardment of the passivated wafer surface, which leads to the deterioration of the cell parameters such as  $V_{oc}$  and  $FF$  [28]. However, the increased lifetime at the power density of as low as  $42 \text{ mW}/\text{cm}^2$  can be akin to a plasma post-treatment in hydrogen environment. Recently, it was argued that the growth of  $\mu\text{c-Si:H}$  material in special high hydrogen dilution can play a similar role as a hydrogen plasma post-treatment [16,17] which is often used to further enhance the surface passivation quality of the wafer [24].

The RE-SHJ designs were implemented, as shown in Fig. 1, to demonstrate the effect of the seed layers on the cell parameters. Fig. 5a shows the light J-V curve characteristics of cells. In addition, the cell parameters, including  $V_{oc}$ ,  $J_{sc}$ ,  $FF$ , and efficiency ( $E_{ff}$ ), extracted from

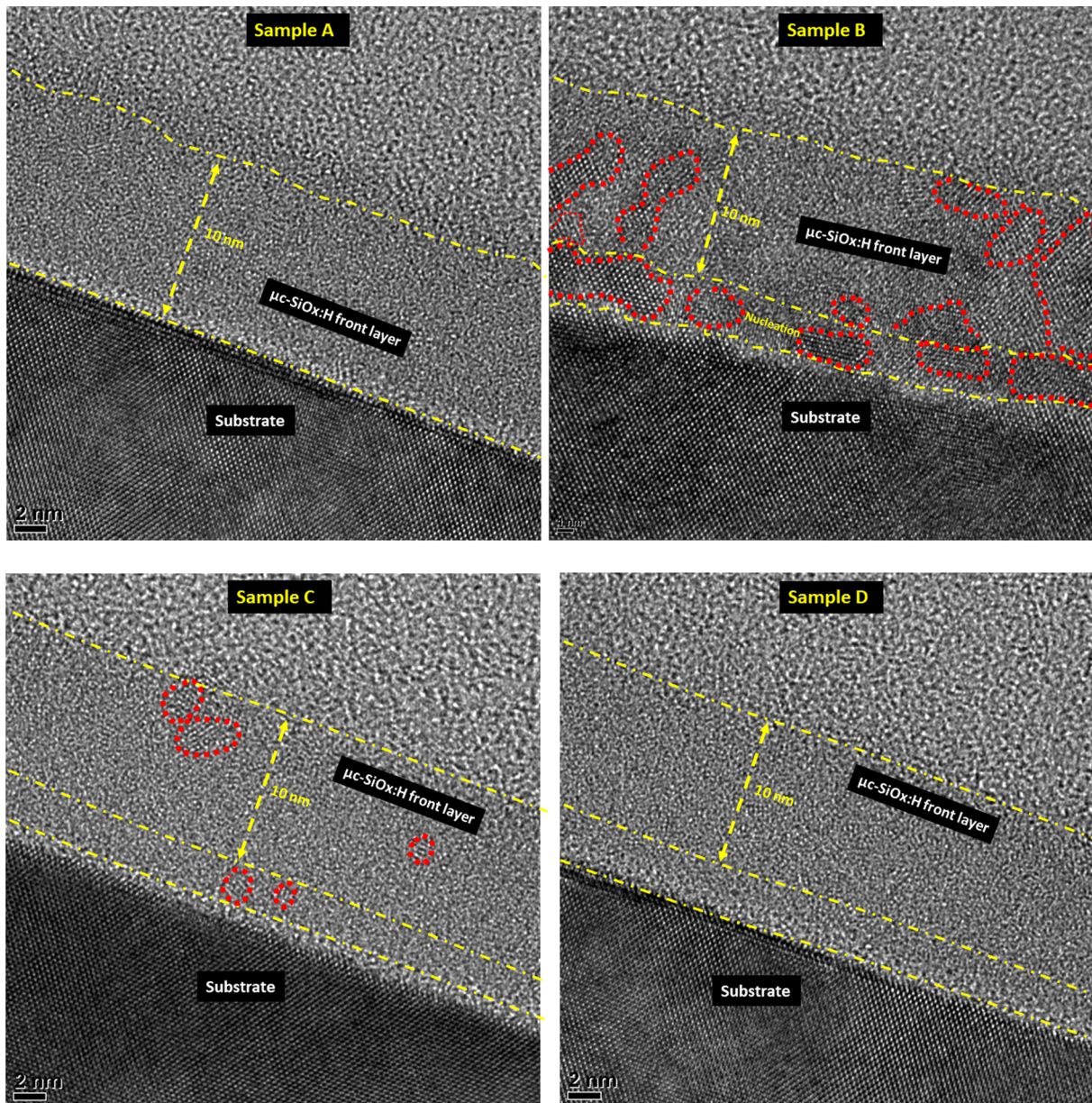


**Fig. 3.** Cross-sectional TEM images of n- $\mu\text{c-SiO}_x\text{:H}$  front layers (sample A–D) deposited on polished wafers. The yellow lines highlight the boundaries of layers including wafer substrate, crystalline nucleation, and n- $\mu\text{c-SiO}_x\text{:H}$  front layer; and the red lines show crystalline phase. (For interpretation of the references to colour in this figure legend, the reader is referred to the web version of this article.)

the light  $I$ - $V$  curve results are shown in Fig. 5b. Whereas the  $J_{sc}$  values were nearly similar, the  $V_{oc}$  and  $FF$  of cell B with a seed layer deposited at  $42 \text{ mW/cm}^2$  were 6 mV and 4.11%, respectively, higher than those of cell A without the seed layer, which resulted in high cell performance of 21.1%. However, these values gradually decreased with the power density of the seed layers. The remarkable increase in the  $V_{oc}$  of cell B was most probably due to the seed-layer-specific PECVD condition, i.e. under a very high hydrogen dilution, which may have acted as a hydrogen-plasma treatment that better enhanced the surface-passivation quality [16,29,30]. The gradual decrease in  $V_{oc}$  with higher power density can be explained by the surface bombardment, as previously mentioned. In particular, it was attributed to the significant enhancement in the crystalline phase as well as the conductivity of the n- $\mu\text{c-SiO}_x\text{:H}$

$\text{SiO}_x\text{:H}$  front contact layer of cell B compared with those of cell A, as shown in Fig. 2 and Table 2, which may have played an important role in the  $FF$  improvement. Fig. 5b clearly shows that the series resistance ( $R_s$ ) of cell B was reduced to 64% compared with that of cell A. These resistances increased with the power densities. The results emphasised that the high-crystalline form of the front contact layers played an important role in the carrier extraction and possibly reduced the series resistance, resulting in high  $FF$ .

#### 4. Conclusion

In conclusion, we have investigated the effects of using various 3 nm seed layers on the crystallinity and conductivity of 10 nm n- $\mu\text{c-SiO}_x\text{:H}$

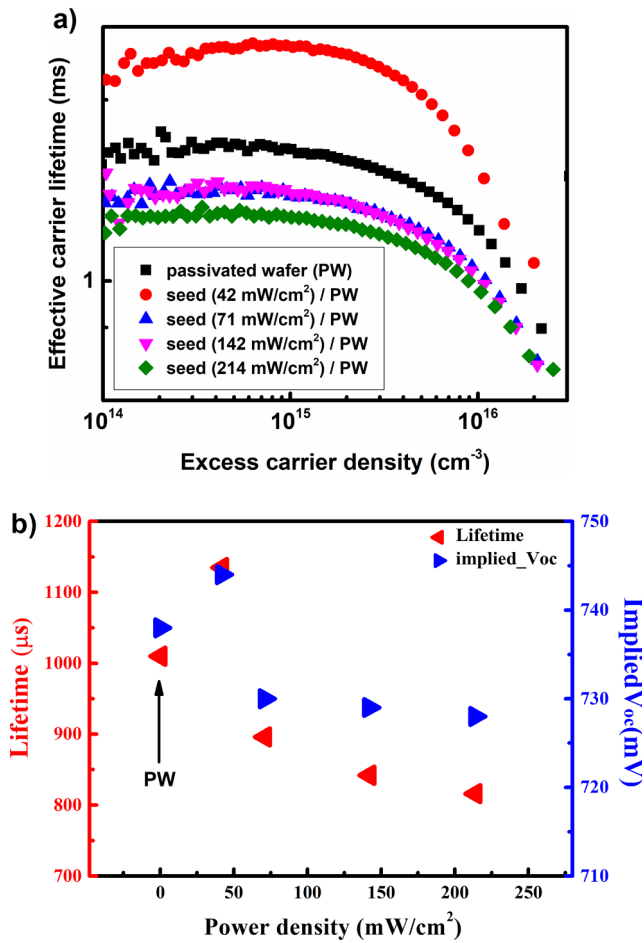


Fig. 4. (a) Effective minority carrier lifetime data and (b) detailed lifetime and implied  $V_{oc}$  values at 1 sun illumination of the passivating structures, including i-layer/textured wafer/i-layer (PW) and i-layer/textured wafer/i-layer/seed layers, as a function of power densities of seed layers.

front contact layers for rear-emitter SHJ solar cells. Using an optimised seed layer, we demonstrated the significant enhancement in the crystalline phase and conductivity of the front window layer. The application of the seed/front window layer stack, with the seed layer prepared at power density of 42 mW/cm<sup>2</sup>, in the rear-emitter SHJ solar cells resulted in enhancement of 6 mV and 4.11% in  $V_{oc}$  and FF, respectively. The improvement in  $V_{oc}$  can be attributed to the seed-layer-specific PECVD condition under high hydrogen dilution, which may have acted as a post-hydrogen treatment for achieving a higher passivation wafer-surface quality. In addition, the enhancement in FF was attributed to the high-crystalline phase and conductivity of the n- $\mu$ c-SiO<sub>x</sub>:H front layer, which resulted in better carrier extraction and lower device series resistance. A high cell performance of 21.1% was obtained.

**Declaration of Competing Interest**

The authors declared that there is no conflict of interest.

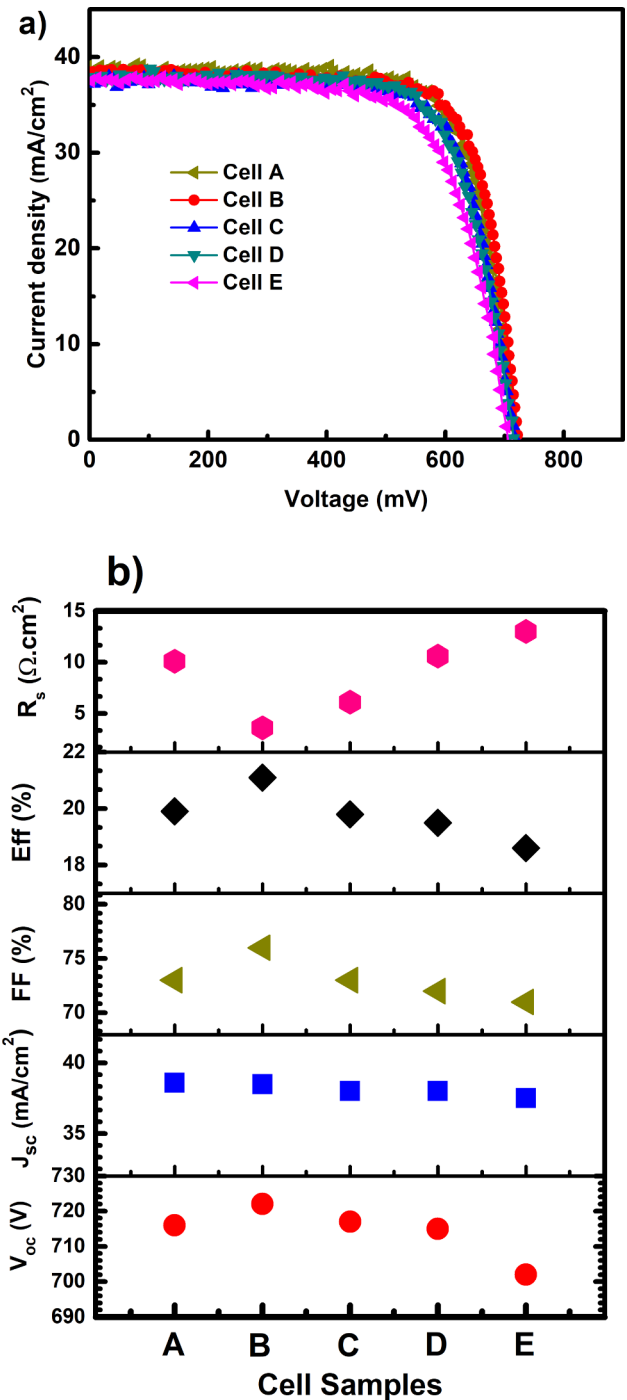


Fig. 5. (a) J-V curve characteristics and (b) cell parameters extracted from I-V curves including  $V_{oc}$ ,  $J_{sc}$ , FF, Eff and  $R_s$  of RE-SHJ cells.

**Acknowledgments**

This work was supported by the National Research Foundation of Korea (NRF) grant funded by the Korea Government (MSIT) (No. 2019R1A2C1009126). This work was also supported by the New & Renewable Energy Core Technology Program of the Korea Institute of

Energy Technology Evaluation and Planning (KETEP), granted financial resource from the Ministry of Trade, Industry & Energy, Republic of Korea (No. 20163010012230).

## References

- [1] M. Taguchi, A. Yano, S. Tohoda, K. Matsuyama, Y. Nakamura, T. Nishiwaki, K. Fujita, E. Maruyama, 24.7% record efficiency HIT solar cell on thin silicon wafer, *IEEE J. Photovolt.* 4 (1) (2014) 96.
- [2] K. Masuko, M. Shigematsu, T. Hashiguchi, D. Fujishima, M. Kai, N. Yoshimura, T. Yamaguchi, Y. Ichihashi, T. Mishima, N. Matsubara, T. Yamanishi, T. Takahama, M. Taguchi, E. Maruyama, S. Okamoto, Achievement of more than 25% conversion efficiency with crystalline silicon heterojunction solar cell, *IEEE J. Photovolt.* 4 (6) (2014) 1433.
- [3] S. De Wolf, A. Descoedres, Z.C. Holman, C. Ballif, High-efficiency silicon heterojunction solar cells: a review, *Green* 2(1) (2012).
- [4] D. Adachi, J.L. Hernández, K. Yamamoto, Impact of carrier recombination on fill factor for large area heterojunction crystalline silicon solar cell with 25.1% efficiency, *Appl. Phys. Lett.* 107 (23) (2015).
- [5] J.L. Hernández, K. Yoshikawa, A. Feltrin, N. Menou, N. Valckx, E.V. Assche, D. Schroos, K. Vandersmissen, H. Philipsen, J. Poortmans, D. Adachi, M. Yoshimi, T. Uto, H. Uzu, T. Kuchiyama, C. Allebé, N. Nakanishi, T. Terashita, T. Fujimoto, G. Koizumi, K. Yamamoto, High efficiency silver-free heterojunction silicon solar cell, *Jpn. J. Appl. Phys.* 51 (2012) 10NA04.
- [6] Z.C. Holman, A. Descoedres, L. Barraud, F.Z. Fernandez, J.P. Seif, S.D. Wolf, C. Ballif, Current losses at the front of silicon heterojunction solar cells, *IEEE J. Photovolt.* 2 (1) (2012) 7–15.
- [7] H. Fujiwara, M. Kondo, Effects of a-Si: H layer thicknesses on the performance of a-Si:H/c-Si heterojunction solar cells, *J. Appl. Phys.* 101 (5) (2007) 054516.
- [8] S. Kim, J. Park, P.D. Phong, C. Shin, S.M. Iftiqar, J. Yi, Improving the efficiency of rear emitter silicon solar cell using an optimized n-type silicon oxide front surface field layer, *Sci. Rep.* 8 (1) (2018) 10657.
- [9] C. Leendertz, N. Mingirulli, T.F. Schulze, J.P. Kleider, B. Rech, L. Korte, Discerning passivation mechanisms at a-Si:H/c-Si interfaces by means of photoconductance measurements, *Appl. Phys. Lett.* 98 (20) (2011) 202108.
- [10] M. Bivour, S. Schröer, M. Hermle, Numerical analysis of electrical TCO/a-Si:H(p) contact properties for silicon heterojunction solar cells, *Energy Procedia* 38 (2013) 658–669.
- [11] K.-U. Ritzau, M. Bivour, S. Schröer, H. Steinkemper, P. Reinecke, F. Wagner, M. Hermle, TCO work function related transport losses at the a-Si:H/TCO-contact in SHJ solar cells, *Sol. Energy Mater. Sol. Cells* 131 (2014) 9–13.
- [12] M. Bivour, C. Reichel, M. Hermle, S.W. Glunz, Improving the a-Si:H(p) rear emitter contact of n-type silicon solar cells, *Sol. Energy Mater. Sol. Cells* 106 (2012) 11–16.
- [13] E. Kobayashi, N. Nakamura, K. Hashimoto, Y. Watabe, Rear-emitter silicon heterojunction solar cells with efficiency above 22%, in: 28th European Photovoltaic Solar Energy Conference and Exhibition, Paris, 2013, pp. 691–694.
- [14] M. Bivour, S. Schröer, M. Hermle, S.W. Glunz, Silicon heterojunction rear emitter solar cells: Less restrictions on the optoelectrical properties of front side TCOs, *Sol. Energy Mater. Sol. Cells* 122 (2014) 120–129.
- [15] M. Bivour, H. Steinkemper, J. Jeurink, S. Schröer, M. Hermle, Rear emitter silicon heterojunction solar cells: fewer restrictions on the optoelectrical properties of front side TCOs, *Energy Procedia* 55 (2014) 229–234.
- [16] L. Mazzarella, A.B. Morales-Vilches, L. Korte, R. Schlatmann, B. Stannowski, Ultra-thin nanocrystalline n-type silicon oxide front contact layers for rear-emitter silicon heterojunction solar cells, *Sol. Energy Mater. Sol. Cells* 179 (2018) 386–391.
- [17] L. Mazzarella, A.B. Morales-Vilches, M. Hendrichs, S. Kirner, L. Korte, R. Schlatmann, B. Stannowski, Nanocrystalline n-type silicon oxide front contacts for silicon heterojunction solar cells: photocurrent enhancement on planar and textured substrates, *IEEE J. Photovolt.* 8 (1) (2017) 70–78.
- [18] A.B. Morales-Vilches, L. Mazzarella, M. Hendrichs, L. Korte, R. Schlatmann, B. Stannowski, Nanocrystalline vs. amorphous n-type silicon front surface field layers in silicon heterojunction solar cells: Role of thickness and oxygen content, in: Proceedings of the 33rd European Photovoltaic Solar Energy Conference and Exhibition, Amsterdam, 2017, 715–719.
- [19] A. Richter, V. Smirnov, A. Lambert, K. Nomoto, K. Welter, K. Ding, Versatility of doped nanocrystalline silicon oxide for applications in silicon thin-film and heterojunction solar cells, *Sol. Energy Mater. Sol. Cells* 174 (2018) 196–201.
- [20] P. Cuony, D.T. Alexander, I. Perez-Wurfl, M. Despeisse, G. Bugnon, M. Boccard, T. Soderstrom, A. Hessler-Wyser, C. Hebert, C. Ballif, Silicon filaments in silicon oxide for next-generation photovoltaics, *Adv. Mater.* 24 (9) (2012) 1182–1186.
- [21] S. Lee, S. Park, J. Park, Y. Kim, K. Yoon, C. Shin, S. Baek, J. Kim, Y.-J. Lee, J. Yi, The effect of carrier injection stress on boron-doped amorphous silicon suboxide layers investigated by X-ray photoelectron spectroscopy, *Jpn. J. Appl. Phys.* 50 (9) (2011) 095801.
- [22] A. Matsuda, Growth mechanism of microcrystalline silicon obtained from reactive plasma, *Thin Solid Films* 337 (1999) 1–6.
- [23] R.W. Collins, A.S. Ferlauto, G.M. Ferreira, C. Chen, J. Koh, R.J. Koval, Y. Lee, J.M. Pearce, C.R. Wronski, Evolution of microstructure and phase in amorphous, protocrystalline, and microcrystalline silicon studied by real time spectroscopic ellipsometry, *Sol. Energy Mater. Sol. Cells* 78 (1–4) (2003) 143–180.
- [24] H. Yue, A. Wu, X. Zhang, T. Li, New two-step growth of microcrystalline silicon thin films without incubation layer, *J. Cryst. Growth* 322 (1) (2011) 1–5.
- [25] Y.-B. Chung, D.-K. Lee, J.-S. Lim, N.-M. Hwang, Reduction of amorphous incubation layer by HCl addition during deposition of microcrystalline silicon by hot-wire chemical vapor deposition, *Sol. Energy Mater. Sol. Cells* 95 (1) (2011) 211–214.
- [26] M. Kondo, M. Fukawa, L. Guo, A. Matsuda, High rate growth of microcrystalline silicon at low temperatures, *J. Non-Cryst. Solids* 266–269 (2000) 84–89.
- [27] A. Matsuda, Formation kinetics and control of microcrystalline in  $\mu$ -Si: H from glow discharge plasma, *J. Non-Cryst. Solids* 59–60 (1983) 767–774.
- [28] S. Kim, V. Ai Dao, Y. Lee, C. Shin, J. Park, J. Cho, J. Yi, Processed optimization for excellent interface passivation quality of amorphous/crystalline silicon solar cells, *Sol. Energy Mater. Sol. Cells* 117 (2013) 174–177.
- [29] M. Mews, T.F. Schulze, N. Mingirulli, L. Korte, Hydrogen plasma treatments for passivation of amorphous-crystalline silicon-heterojunctions on surfaces promoting epitaxy, *Appl. Phys. Lett.* 102 (12) (2013) 122106.
- [30] A. Descoedres, L. Barraud, S. De Wolf, B. Strahm, D. Lachenal, C. Guérin, Z.C. Holman, F. Zicarelli, B. Demareux, J. Seif, J. Holovsky, C. Ballif, Improved amorphous/crystalline silicon interface passivation by hydrogen plasma treatment, *Appl. Phys. Lett.* 99 (12) (2011) 123506.